Journal of Solid State Chemistry **156,** 355–363 (2001)
doi:10.1006/jssc.2000.9006, available online at http://www.idealibrary.com on IDEAL®

Oxygen Nonstoichiometry, Structures, and Physical Properties of $YBaCo_2O_{5+x}$ ($0.00 \leq x \leq 0.52$)

D. Akahoshi and Y. Ueda

Materials Design and Characterization Laboratory, Institute for Solid State Physics, The University of Tokyo, Kashiwanoha, Kashiwa-shi, Chiba, 277-8581, Japan

Received June 29, 2000; in revised form October 5, 2000; accepted October 13, 2000; published online January 3, 2001

We synthesized $YBaCo_2O_{5+x}$ with various oxygen contents x and investigated physical and structural properties. $YBaCo_2O_{5+x}$ can be classified into three parts of composition region in the structural properties. Two kinds of superstructure, $2 \times 1 \times 1$ and $3 \times 3 \times 1$, originating in the ordering of excess oxygen in $Y(O)_x$ layer appear in the range $0.50 \leq x$ and $0.25 \leq x \leq 0.44$, respectively. The $2 \times 1 \times 1$ phase shows the metal–insulator transition accompanied with the large lattice distortion and the magnetic transition. The $3 \times 3 \times 1$ phase (stoichiometric composition, $x = 0.44$) also shows some magnetic and structural transitions. A plausible model of the $3 \times 3 \times 1$ superstructure is proposed. In the range $0.00 \leq x \leq 0.19$, $YBaCo_2O_{5+x}$ has no longer superstructure. $YBaCo_2O_{5+x}$ in $x = 0.00$ shows successive phase transitions, a paramagnetic tetragonal to antiferromagnetic orthorhombic transition, and a charge order transition. The present study reveals a simultaneous phase separation with the charge order transition.

Key Words: **oxygen nonstoichiometry; superstructure; metal–insulator transition; magnetic transition; structural transition; charge order; phase separation; phase diagram.**

INTRODUCTION

The 3d transition-metal oxides with perovskite-type structure show a wide variety of physical and structural properties. Therefore, they have been intensively investigated up to now. Among these oxides, especially copper and manganese oxides have attracted considerable attention for high-T_C superconductivity and colossal magnetoresistance (CMR) effect, respectively.

Recently, physical and structural properties of new cobalt oxides, $RBaCo_2O_{5+x}$ (R = Y, Pr, Nd, Sm, Eu, Gd, Tb, Dy, and Ho) were reported by some groups (1–8). These new cobalt oxides have a wide range of oxygen nonstoichiometry, and they show attractive electromagnetic and structural properties depending on the oxygen nonstoichiometry.

$RBaCo_2O_{5+x}$ has a 112-type structure, that is, an oxygen-deficient and A-site ordered perovskite. Figure 1a shows the crystal structure of $YBaCo_2O_{5+x}$ ($x = 0.00$). The structure is achieved by stacking BaO, CoO_2, Y, CoO_2, and BaO layers along the c-axis in this order, and all Co atoms are in square pyramidal coordination. These CoO_5 square pyramids are connected with each other through the corners, and consequently two-dimensional Co_2O_5 block layers are formed. Moreover, as clearly seen in Fig. 1a, $YBaCo_2O_{5+x}$ ($x = 0.00$) has the characteristic CoO_2–Y–CoO_2 block layer similar to CuO_2–Y–CuO_2 block layer playing an important role in high-T_C superconductivity of $YBa_2Cu_3O_{6+x}$ (YBCO). The average valence of Co ions is 2.5 + with a mix-valence state of Co^{2+} and Co^{3+}. Here it is worth noting that Co ions of $YBaCo_2O_{5+x}$ ($x = 0.00$) are in a unique oxygen-coordination of square pyramid but a mix-valence state of Co^{2+} and Co^{3+}. Previously, we first reported some kind of phase transition at around 220 K in $YBaCo_2O_{5+x}$ ($x = 0.0$) (3), and recently Vogt *et al.* reported a simultaneous Néel order with a tetragonal–orthorhombic transition at 330 K and a charge order transition at 220 K (8).

$RBaCo_2O_{5+x}$ can accommodate excess-oxygen atoms in the $R(O)_x$ layer differing from YBCO, and the oxygen nonstoichiometry (the oxygen content x) is attributed to the occupancy rate of oxygen sites in $R(O)_x$ layer. The oxygen content x is sensitive to temperature and atmosphere (oxygen-partial-pressure) and is variable between about 0.0 and 0.7. The maximum value of x is dependent on the size of R^{3+} and increases with an increase of the size of R^{3+} (e.g., Pr, $x = 0.7$; Ho, $x = 0.3$; they were synthesized in air (5)). Because of the wide range of oxygen nonstoichiometry, several types of superstructures are expected in various manners of arraying oxygen atoms in $R(O)_x$ layer. In fact, two kinds of superstructures, $3 \times 3 \times 1$ and $2 \times 1 \times 1$, have been reported (1–5). Figure 1b shows an ideal $2 \times 1 \times 1$ superstructure in $YBaCo_2O_{5+x}$ (stoichiometric composition, $x = 0.50$). As seen in Fig. 1b, half Co atoms are in octahedral coordination, and the other half in square pyramidal coordination. Furthermore, an alternative appearance of one-dimensional CoO_6 octahedral and CoO_5 square pyramidal chains running along the b-axis produces

0022-4596/01 $35.00

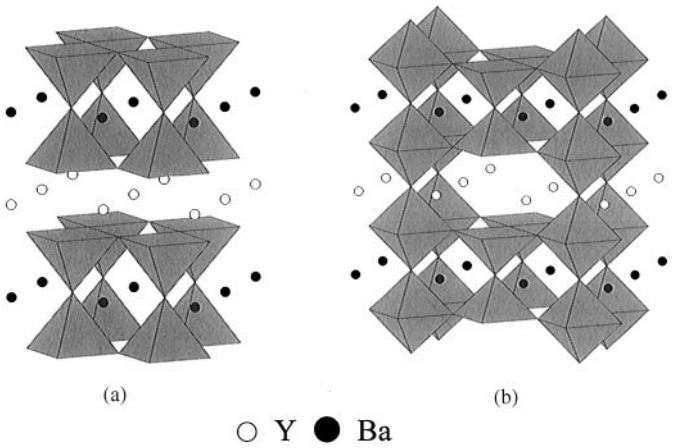

FIG. 1. Schematic crystal structures of (a) $YBaCo_2O_{5.00}$ and (b) $YBaCo_2O_{5.50}$ with $2\times1\times1$ superstructure. Large open and filled circles indicate Y and Ba, respectively. All Co atoms are in square pyramidal coordination in (a). Half Co atoms are in square pyramidal coordination and the other half in octahedral coordination in (b).

the $2\times1\times1$ superstructure, and the average valence of Co ions is 3.0 + . Here it should be noted again that Co ions of $YBaCo_2O_{5+x}$ ($x = 0.50$) are in two kinds of oxygen-coordination (octahedra and square pyramid) but in a single valence state of Co^{3+} in contrast to $YBaCo_2O_{5+x}$ ($x = 0.00$).

As for physical properties, $RBaCo_2O_{5+x}$ with the $2\times1\times1$ superstructure shows a metal–insulator (M–I) transition and magnetoresistance (MR) effect (3–7). The MR effect in the cobalt oxides with perovskite structure has been reported in $La_xSr_{1-x}CoO_3$ (9–11). Therefore, it is interesting to compare $RBaCo_2O_{5+x}$ with $La_xSr_{1-x}CoO_3$ in terms of the structure and physical properties. $RBaCo_2O_{5+x}$ also exhibits several magnetic transitions. However, magnetic ions in *A*-site such as Gd, Tb make magnetic behaviors of $RBaCo_2O_{5+x}$ rather complicated because of the magnetic properties of *A*-ions themselves. Since Y^{3+} is a nonmagnetic ion, $YBaCo_2O_{5+x}$ is a good example for investigating physical properties of Co ion itself in $RBaCo_2O_{5+x}$.

As mentioned above, $RBaCo_2O_{5+x}$ shows a variety of structural and physical properties with a change of *x*. Therefore, to understand $RBaCo_2O_{5+x}$, a detailed study is required on the relations between *x* and the structure, physical properties. Nevertheless, there is no study like that at present. We synthesized $YBaCo_2O_{5+x}$ with various oxygen contents *x* and investigated their structures and physical properties. We report the detailed phase diagram of $YBaCo_2O_{5+x}$ as functions of *x* and temperature in this article.

EXPERIMENTAL

$YBaCo_2O_{5+x}$ was prepared by a solid-state reaction using Y_2O_3, $BaCO_3$, and CoO as starting materials. Mixed powder of starting materials in appropriate molar ratios was ground, pressed into pellets and heated at 1273 K in pure oxygen gas for one day, and then this procedure was repeated several times to remove impurity phases. Finally, the sample was cooled from 1273 K to room temperature at the rate of about 100 K/h. The sample thus obtained has the oxygen content of $x = 0.50$ and an orthorhombic structure with the $2\times1\times1$-superstructure.

The following method was employed to obtain $YBaCo_2O_{5+x}$ with various oxygen contents *x*. We performed thermogravimetric (TG) analysis of the $x = 0.50$ sample under various atmosphere. Since oxygen-release or -absorption starts at around 550 K, we prepared the samples with the desired *x* value by choosing appropriate annealing temperature and atmosphere. The sample with $x = 0.52$ was obtained by annealing the $x = 0.50$ sample under high oxygen pressure (100 atm) at 573 K for several hours. The $x = 0.44$ sample was obtained by annealing the $x = 0.50$ sample under an oxygen atmosphere at 563 K for several hours and then cooling it rapidly to room temperature. The sample with $x = 0.40$ (0.35, 0.25, 0.19, 0.15, 0.08, 0.03, and 0.00) was obtained by heating the $x = 0.50$ sample in pure argon gas up to 553 K (563, 593, 613, 633, 693, 973, and 1023 K) and then cooling it to room temperature at the rate of 1 K/min.

Sample characterization and observation of structural transition were performed by X-ray powder diffraction (XPD) using a Mac Science MXP21 system with a rotating anode generator, a monochromator of single crystalline graphite for Cu$K\alpha$ radiation, and a refrigerator. The synthesized samples included unknown impurities, but the amount of them was negligible.

The oxygen content *x* was directly determined by the following method. $YBaCo_2O_{5+x}$ treated under hydrogen atmosphere at 1273 K was decomposed into Y_2O_3, BaO, and Co-metal, and *x* was determined from an amount of the weight loss detected by TG analysis.

Magnetic properties were studied with a Quantum Design MPMS SQUID magnetometer in the temperature range from 5 to 350 K. The $x = 0.00$ sample was sealed in an evacuated silica tube and measured in the temperature range from 5 to 700 K. Differential scanning calorimetric (DSC) measurements were performed at the rate of 10 K/min in a Mac Science DSC 3200S in the temperature range from 150 to 400 K. Resistivity was measured by an ordinary four-probe method.

RESULTS AND DISCUSSION

In Table 1, we collect oxygen contents, lattice parameters at room temperature, and synthesis conditions of samples prepared in this study. $YBaCo_2O_{5+x}$ can be classified into three parts of composition region in the structural properties as described below.

TABLE 1
Synthesis Conditions and Lattice Parameters of $YBaCo_2O_{5+x}$ at Room Temperature

Oxygen content	a (Å)	b (Å)	c (Å)	Synthesis conditions
$2\times1\times1$ Superstructure				
$x = 0.52$	2×3.923	3.819	7.516	SC from 573 K in O_2 (100 atm)
$x = 0.50$	2×3.923	3.819	7.516	SC from 1273 K in O_2
$3\times3\times1$ Superstructure				
$x = 0.44$	3×3.872	(tetra)	7.502	RC from 563 K in O_2
$x = 0.40$	3×3.872	(tetra)	7.499	SC from 553 K in Ar
$x = 0.35$	3×3.874	(tetra)	7.497	SC from 563 K in Ar
$x = 0.25$	3×3.875	(tetra)	7.498	SC from 593 K in Ar
No superstructure				
$x = 0.19$	3.878	(tetra)	7.495	SC from 613 K in Ar
$x = 0.15$	3.881	(tetra)	7.492	SC from 633 K in Ar
$x = 0.08$	3.886	3.885	7.480	SC from 693 K in Ar
$x = 0.03$	3.889	3.886	7.481	SC from 973 K in Ar
$x = 0.00$	3.892	3.887	7.476	SC from 1023 K in Ar

Note. SC, slow cooling; RC, rapid cooling.

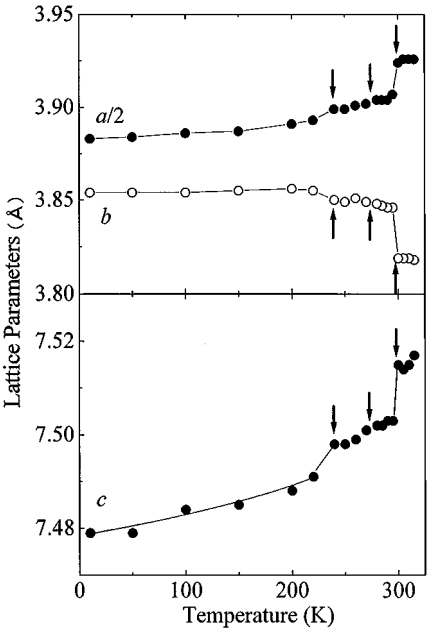

FIG. 3. Temperature dependence of lattice parameters of $YBaCo_2O_{5.50}$ (heating process).

(1) Samples with $0.50 \le x$

In this region, we synthesized two samples, $x = 0.50$ and 0.52. The crystal structures of them are orthorhombic ones with the $2\times1\times1$ superstructure. We first reported the $2\times1\times1$ superstructure in $x = 0.50$ in the previous paper (3). In the present study, the $2\times1\times1$ superstructure was confirmed by both XPD and electron diffraction (ED) measurements. It is clear that the orthorhombic distortion is due to the oxygen ordering in $Y(O)_x$ layer (see Fig. 1b). However, ED measurements indicate that the real structure of the $x = 0.50$ sample is more complicated than that shown in Fig. 1b. We are now preparing a report of detailed results of ED measurements. At room temperature, no significant difference of lattice parameters was observed between the $x = 0.50$ and the $x = 0.52$ samples.

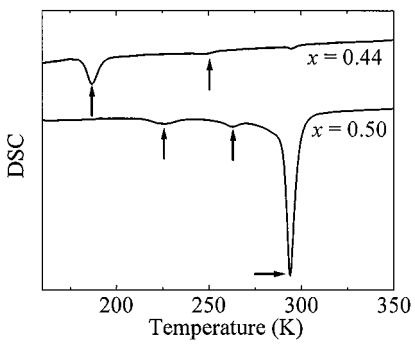

FIG. 2. DSC curves of $YBaCo_2O_{5+x}$ ($x = 0.50$ and 0.44) in heating process.

As previously reported (3), $YBaCo_2O_{5+x}$ ($x = 0.50$) with the $2\times1\times1$ superstructure exhibits successive phase transitions. The DSC curve of the $x = 0.50$ sample in heating process is shown in Fig. 2. It shows three endothermic peaks at around 295, 270, and 230 K, suggesting first-order transitions. The temperature dependence of lattice parameters of the $x = 0.50$ sample (Fig. 3, heating process) shows an abrupt change at around 295 K, that is, the a-axis perpendicular to oxygen chains in $Y(O)_x$ layer (see Fig. 1b) shrinks as well as the c-axis while the b-axis parallel to oxygen chains lengthens, as temperature decreases. A clear anomaly was recognized at around 230 K but not at around 270 K in the temperature dependence of lattice parameters. These results are consistent with a strong DSC peak at 295 K and weak DSC peaks at 270 and 230 K. In spite of the successive three transitions, the crystal structure of the $x = 0.50$ sample remains orthorhombic at low temperature.

We previously reported the magnetic and M–I transitions in $YBaCo_2O_{5+x}$ ($x = 0.50$) with the $2\times1\times1$ superstructure (3). Figure 4a shows the temperature dependence of magnetization and resistivity of the $x = 0.50$ sample measured in heating process. The inset shows a logarithm plot of magnetization around the transition temperature. No significant difference of magnetization was observed between zero field cool (ZFC) and field cool (FC) measurements. As seen in Fig. 4a, the magnetization measured under $H = 0.01$ T seems to increase gradually below 297 K and sharply below 290 K and then decreases suddenly below 270 K. At 230 K where the DSC curve shows a weak peak, the magnetization–temperature (M–T) curve shows no anomaly. The

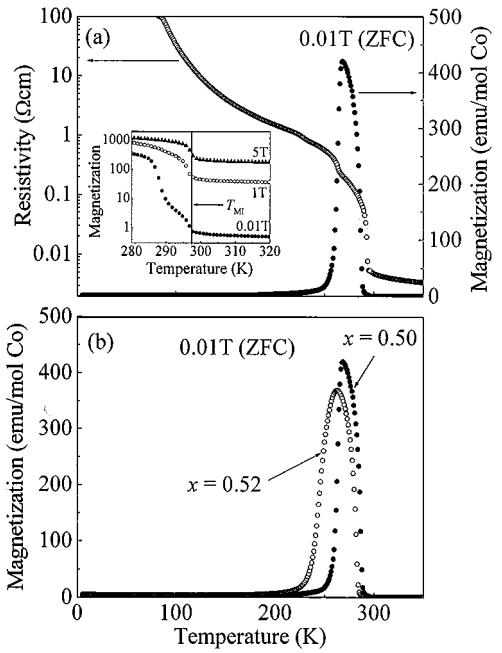

FIG. 4. (a) Temperature dependence of resistivity and magnetization (ZFC) of $YBaCo_2O_{5.50}$. (b) Temperature dependence of magnetization (ZFC) of $YBaCo_2O_{5+x}$ ($x = 0.50$ and 0.52).

magnetization–applied field (M–H) curve at 270 K shows a ferromagnetic behavior, suggesting a paramagnetic (PM) to ferromagnetic (FM) transition at around 290 K. The saturated value of magnetization at 270 K under $H = 5$ T, however, corresponds to about 0.20 μ_B/Co which is much smaller than 4 μ_B/Co, that of high-spin Co^{3+}. Therefore, it is likely that the magnetism of the $x = 0.50$ sample is a weak ferromagnetism (WFM) originating in a canted antiferromagnetism below 290 K (T_{PM-WFM}). The sudden decrease of magnetization below 270 K ($T_{WFM-AFM}$) can be considered to be due to the transition from a canted antiferromagnetism to a normal antiferromagnetism (AFM) where the magnetic moments of cobalt sublattices cancel out with each other, because the M–H curve at 5 K does not show any saturation behavior but does a linear relation up to $H = 5$ T.

The resistivity of the $x = 0.50$ sample (Fig. 4a) shows an abrupt increase below 297 K and a slight increase each at 270 and 230 K. These transition temperatures coincide with those in DSC measurements. At 297 K, the resistivity jumps by about two orders of magnitude. That is, a M–I transition occurs at the temperature. The T_{M-I} agrees well with the temperature where the magnetization begins to gradually increase (see the inset of Fig. 4a) but is somewhat higher than T_{PM-WFM} (290 K). The T_{PM-WFM} was shifted to higher temperature as external magnetic field increased, but the T_{M-I} was not affected by external magnetic fields. The magnetization measured under $H = 1$ T sharply increases below T_{M-I}, as shown in the inset of Fig. 4a, suggesting $T_{M-I} = T_{PM-WFM}$. From these results, it is difficult to conclude whether there exists a correlation between the M–I transition and PM-WFM transition. Both M–I and PM-WFM transitions have been observed in other $RBaCo_2O_{5+x}$ compounds with the $2 \times 1 \times 1$ superstructure (5). In some of them, the T_{M-I} is rather higher than the T_{PM-WFM}. This indicates no correlation between the M–I and PM-WFM transitions. In case of $YBaCo_2O_{5+x}$ ($x = 0.50$), the T_{M-I} accidentally coincides with the T_{PM-WFM}. At T_{M-I}, the charges are localized, and then below T_{M-I}, the magnetic order occurs.

The M-I transition is accompanied with the large change of lattice parameters (see Fig. 3). Above T_{M-I}, the large orthorhombic lattice-distortion caused by the oxygen-ordering may be relaxed by a screening effect of delocalized electrons, but the localization of electrons may lead to a decrease of the orthorhombic lattice distortion. As another possibility, a high-spin to low-spin transition may occur at T_{M-I}. A high-spin state of Co^{3+} atoms could prefer octahedral coordination while a low-spin state, more strictly an intermediate-spin state (t_{2g}^5 and e_g^1) could prefer square pyramidal coordination, and as a result, the a-axis shrinks and the b-axis is elongated. One may expect a charge separation into Co^{2+} and Co^{4+} with different oxygen-coordinations in the insulating phase, because of the observed ferrimagnetic behavior (weak ferromagnetism). However, any evidence for such charge separation has not been observed yet. The anomaly of resistivity–temperature curve at 270 K coincides with the WFM-AFM transition.

A considerable MR effect was observed in $YBaCo_2O_{5+x}$ ($x = 0.50$) just like other $RBaCo_2O_{5+x}$ compounds (4–7). We will discuss the MR effect of $YBaCo_2O_{5+x}$ system in a separate paper that is now in preparation.

Compared with the $x = 0.50$ sample, the T_{PM-WFM} and $T_{WFM-AFM}$ of the $x = 0.52$ sample are slightly low, and the WFM-AFM transition is broadened (Fig. 4b). These are due to a deviation from the stoichiometric composition ($x = 0.50$). As seen from this, magnetic properties are more sensitive to the oxygen content x than the lattice parameters are.

(2) Samples with $0.25 \leq x \leq 0.44$

In this region, we obtained four samples, $x = 0.25$, 0.35, 0.40, and 0.44. Their crystal structures are tetragonal ones with a $3 \times 3 \times 1$-superstructure at room temperature (Table 1). In the range $0.45 \leq x \leq 0.49$, the $2 \times 1 \times 1$- and $3 \times 3 \times 1$-phases inevitably coexist, and samples in single phase could not be obtained.

Zhou *et al.* first reported the $3 \times 3 \times 1$ superstructure (1, 2). There are several possible models for the $3 \times 3 \times 1$ superstructure as illustrated in Fig. 5. The stoichiometric composition is $x = \frac{4}{9} = 0.44$ in the models (a) and (b), $x = \frac{5}{9} = 0.56$ in the models (c) and (d), and $x = \frac{1}{9} = 0.11$ in

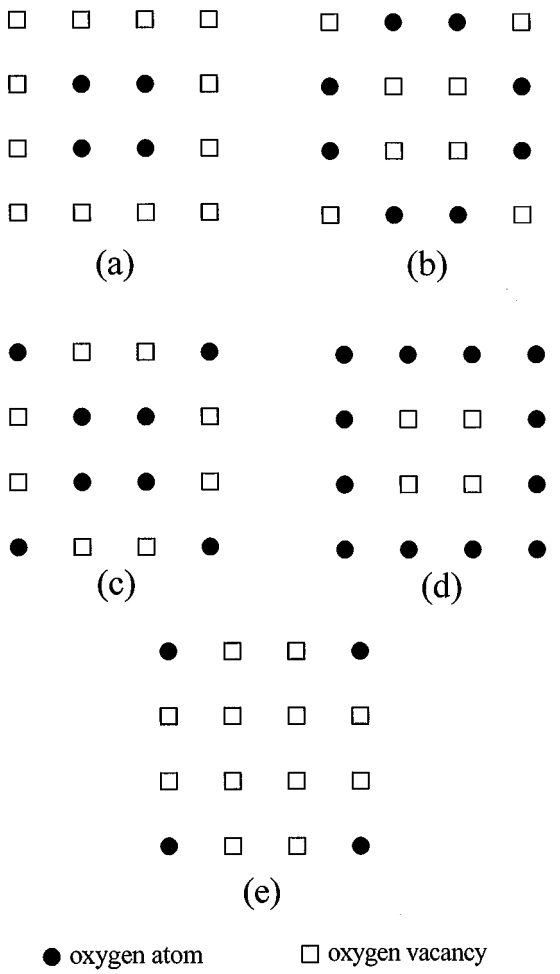

FIG. 5. Models for $3 \times 3 \times 1$ superstructure. The manners of oxygen-ordering in $Y(O)_x$ layer are represented. Y atoms are omitted for convenience.

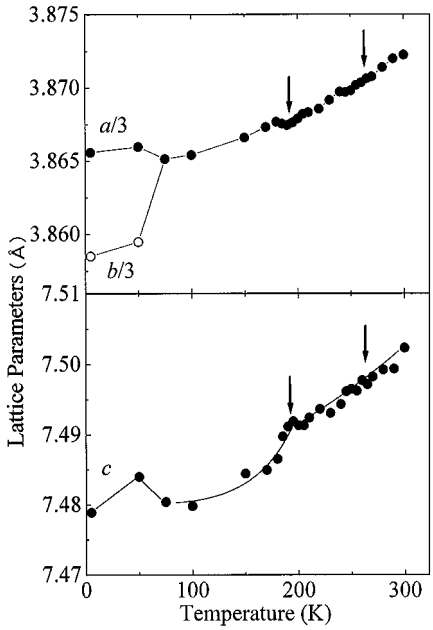

FIG. 6. Temperature dependence of lattice parameters of $YBaCo_2O_{5.44}$ (heating process).

the model (e), respectively. Therefore, the $3 \times 3 \times 1$ phase theoretically exists in the range $0.11 \leq x \leq 0.56$. However, experimentally the phase was found for the range $0.25 \leq x \leq 0.44$. This suggests the model (a) or (b) as a plausible model for the $3 \times 3 \times 1$ superstructure. In the range $0.25 \leq x \leq 0.44$, the superlattice reflection (2/3 0 1) is strongest in $x = 0.44$ and getting weak with a decrease of x, and then it completely disappears in the range $x < 0.25$. Taking these results into account, we can conclude that a model for the $3 \times 3 \times 1$ superstructure is the (a) or (b) type with the stoichiometric composition of $x = 0.44$. The preliminary Rietveld analysis of XPD pattern suggests the (a) type.

The DSC curve of the $x = 0.44$ sample (Fig. 2) indicates the existences of a first-order transition at around 190 K and a second-order transition at around 260 K. The weak DSC peak at around 295 K in the $x = 0.44$ sample can be attributed to the $2 \times 1 \times 1$ phase included accidentally. The temperature dependence of lattice parameters of the $x = 0.44$ sample (Fig. 6) shows an anomaly at 190 K but not a significant change at 260 K. Surprisingly, the $x = 0.44$ sample exhibits a tetragonal–orthorhombic (T–O) transition at around $T_{T-O} = 70$ K. This T–O transition in $x = 0.44$ may be due to rotations of the CoO_6 octahedron units around [001]. The other samples in the $3 \times 3 \times 1$ phase show no T-O transition and remain tetragonal at 5 K.

Figure 7a shows the temperature dependence of magnetization and resistivity of the $x = 0.44$ sample, and they were measured in heating process. The magnetization sharply increases below 260 K and then suddenly decreases below 190 K, and this behavior is similar to that observed in $x = 0.50$ (see Fig. 4a). The resistivity of the $x = 0.44$ sample does not show any change at 260 K, but at 190 K there is a clear jump. The M–H curves indicate a PM-WFM transition at $T_{PM-WFM} = 260$ K and a WFM-AFM transition at $T_{WFM-AFM} = 190$ K. The magnetic moment estimated from M–H curves is about 0.30 μ_B/Co in the WFM state of the $x = 0.44$ sample. The magnetization in FC measurements is slightly different from that in ZFC measurements, and it shows a cluster-glass-like behavior below $\sim$80 K (the inset in Fig. 7a). This behavior may have a relation to the observed T–O transition.

The $3 \times 3 \times 1$ phase is a semiconductor in the measured temperature range. On the other hand, the $2 \times 1 \times 1$ phase of $RBaCo_2O_{5+x}$ (e.g., R = Gd, Eu) was reported to exhibit the M-I transition even at $x = 0.4$ (5). These results indicate that the ordered manner of excess-oxygen atoms in $R(O)_x$ layer is more important for the M-I transition in $RBaCo_2O_{5+x}$ than the oxygen content x or the carrier density.

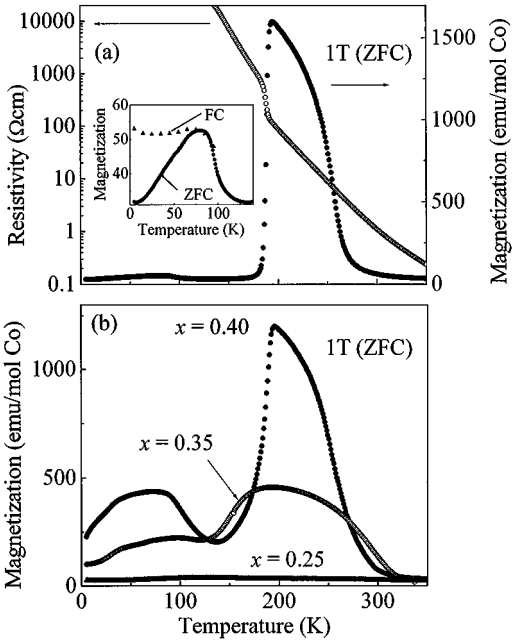

FIG. 7. (a) Temperature dependence of resistivity and magnetization (ZFC) of $YBaCo_2O_{5.44}$. (b) Temperature dependence of magnetization (ZFC) of $YBaCo_2O_{5+x}$ ($x = 0.40$, 0.35, and 0.25).

Figure 7b shows the M–T curves of the $x = 0.40$, 0.35, and 0.25 samples at $H = 1$ T (ZFC, heating process). As x decreases or deviates from the stoichiometric composition ($x = 0.44$), the magnetic behavior becomes more complex and magnetic transitions are broadened and finally disappear. Furthermore, the anomaly of the resistivity at $T_{\mathrm{WFM-AFM}}$ soon disappears with a decrease of x.

(3) Samples with $0.00 \leq x \leq 0.19$

In this region, we synthesized five samples, $x = 0.00$, 0.03, 0.08, 0.15, and 0.19. At room temperature, the samples with $x = 0.00$, 0.03, and 0.08 have orthorhombic primitive cells in the crystal structures, and the samples with $x = 0.15$ and 0.19 have tetragonal primitive cells (Table 1). No superstructure was observed in this region. Probably the reason for this is that the occupancy rate of oxygen sites in $Y(O)_x$ layer are too low to interact with each oxygen atom, and consequently oxygen atoms occupy oxygen sites in $Y(O)_x$ layer at random.

It was found from XPD measurements that the $x = 0.15$ and 0.19 samples which are tetragonal at room temperature exhibit T-O transitions at around $T_{\mathrm{T-O}} = 290$ and 250 K, respectively. Vogt *et al.* reported a T-O transition at around 330 K in $YBaCo_2O_5$ (8). These results indicate that the $T_{\mathrm{T-O}}$ decreases with an increase of the oxygen content x. Figure 8 shows DSC curves of the $x = 0.00$, 0.03, 0.08, 0.15, and 0.19 samples in heating process. The DSC curves of the

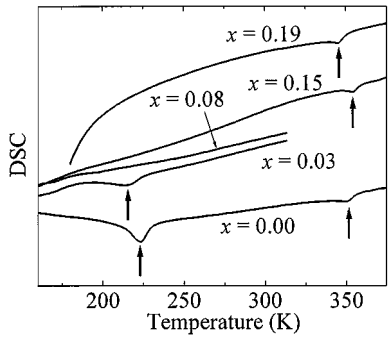

FIG. 8. DSC curves of $YBaCo_2O_{5+x}$ ($x = 0.00$, 0.03, 0.08, 0.15, and 0.19) in heating process.

$x = 0.15$ and 0.19 samples show no anomaly at $T_{\mathrm{T-O}}$, suggesting a second-order character of the T-O transition. The DSC curve of the $x = 0.00$ sample shows a strong endothermic peak at around 220 K and a small one at around 350 K. The M–T curve of the $x = 0.00$ sample shows an anomaly at around 350 K, as shown in Fig. 9, agreeing with the data reported before (8). Vogt *et al.* reported that a paramagnetic-antiferromagnetic (PM-AFM) and T-O transitions simultaneously occur at around 330 K in $YBaCo_2O_5$ (8). Therefore, the observed DSC peak and an anomaly of magnetization at 350 K may be attributed to the paramagnetic tetragonal to antiferromagnetic orthorhombic transition. However, a similar DSC peak was observed at almost the same temperature (350 K) even in $x = 0.19$, as shown in Fig. 8. The T-O transition in $x = 0.19$ occurs at around 250 K, as mentioned above. Therefore, we can conclude that the DSC peak at 350 K can be attributed to the PM-AFM transition, and the T-O transition accidentally coincides with the PM-AFM transition in $x = 0.00$. The T-O transition is sensitive to the oxygen content x, but the PM-AFM transition is insensitive to it.

We previously reported some kind of phase transition at around 220 K in $x = 0.00$, accompanied with a reduction of

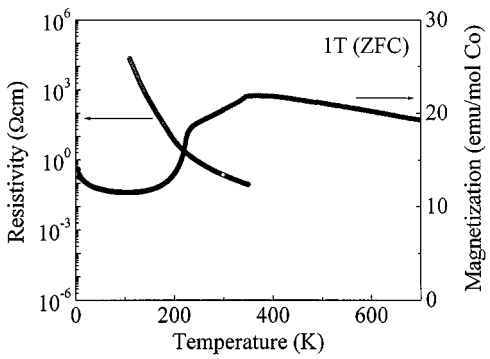

FIG. 9. Temperature dependence of resistivity and magnetization (ZFC) of $YBaCo_2O_{5.00}$.

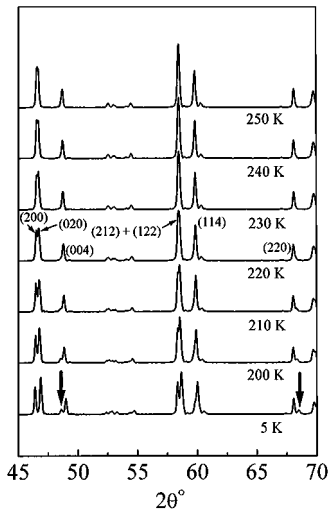

FIG. 10. X-ray diffraction patterns of $YBaCo_2O_{5.00}$ taken at various temperatures.

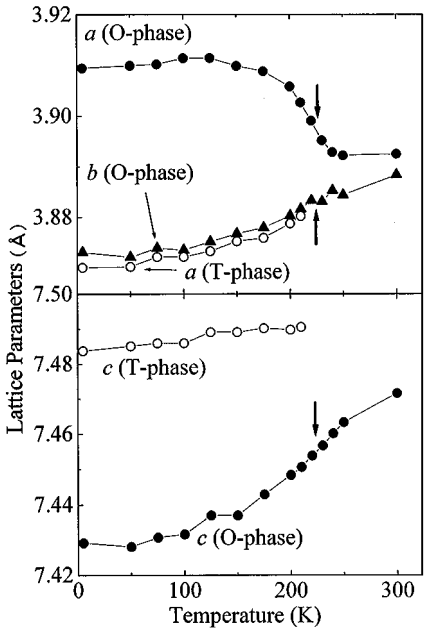

FIG. 11. Temperature dependence of lattice parameters of $YBaCo_2O_{5.00}$ (heating process).

magnetization and a slight change of resistivity (3). Recently, Vogt *et al.* reported a Co^{2+}/Co^{3+} charge ordering as well as a change in the Co^{2+} spin state from high to low spin at $T_{CO} = 220$ K (8). They also reported an increase of orthorhombic distortion below 220 K. We carefully measured XPD in the temperature range from 5 to 300 K. The XPD pattern of the $x = 0.00$ sample shows a complex change below 220 K (Fig. 10). Below the temperature, some reflections are split, and furthermore additional peaks appear in the lower 2θ side of (002), (003), and (004) reflections and in the higher 2θ side of (110) and (220) reflections, as seen in Fig. 10. This behavior is reproducible across the transition. The XPD pattern of the low temperature phase ($T < 220$ K) seems not to be indexed as an orthorhombic or any other structures with lower symmetries, but it can be interpreted as a superposition of two phases, an orthorhombic phase (O-phase) and a tetragonal phase (T-phase).

This suggests a phase separation below 220 K, and the ratio of amount of the T-phase to the O-phase is estimated to be about $\frac{1}{5}$. Figure 11 shows the temperature dependence of lattice parameters of the two phases ($x = 0.00$ sample). The orthorhombic distortion of the O-phase, especially the *a*-axis, abruptly increases below 220 K. On the other hand, the *a*-axis of the T-phase is almost equal to the *b*-axis of the O-phase, and the *c*-axis of the T-phase is much larger than that of the O-phase. Vogt *et al.* observed a similar increase of the orthorhombic distortion due to a charge ordering but not a phase separation (8). We have no explanation for this discrepancy at present. As described below, the phase separation is very sensitive to the oxygen content *x*. The sample Vogt *et al.* used may be slightly in off-stoichiometry or have slight excess-oxygen.

The DSC peak becomes weak in $x = 0.03$ and invisible in $x = 0.08$ (see Fig. 8), although the transition temperature seems not to depend on *x* significantly. As seen from the result, this transition, especially the phase separation is very sensitive to the oxygen content *x*. The coexistence of the O- and T-phases below 220 K can be barely recognized in the XPD pattern of the $x = 0.03$ sample but no longer in that of the $x = 0.08$ sample. As mentioned above, the increase of the orthorhombic distortion is characteristic of the transition. Figure 12 shows the orthorhombicity defined as $2(a - b)/(a + b)$ as a function of T/T_{T-O} where T_{T-O} of each samples is 350 K ($x = 0.00$), 340 K ($x = 0.03$), 320 K ($x = 0.08$), and 290 K ($x = 0.15$), respectively. The abrupt increase of the orthorhombicity can be clearly seen in $x = 0.00$, 0.03, and 0.08. Therefore, we conclude that the phase boundary lies between $x = 0.08$ and $x = 0.15$. This

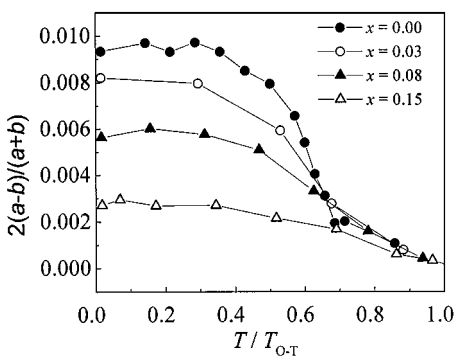

FIG. 12. Temperature dependence of orthorhombicity of $YBaCo_2O_{5+x}$ ($x = 0.00$, 0.03, 0.08, and 0.15).

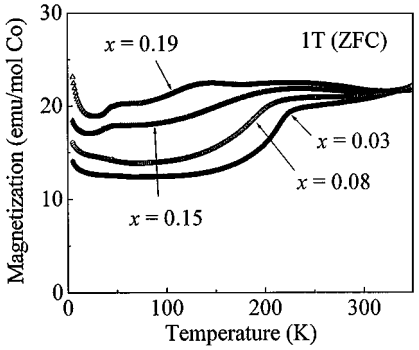

FIG. 13. Temperature dependence of magnetization (ZFC) of $YBaCo_2O_{5+x}$ ($x = 0.03$, 0.08, 0.15, and 0.19).

conclusion can be deduced from the M–T curves. The reduction of magnetization at around 220 K can be clearly observed in $x = 0.00$, 0.03, and 0.08 but no longer clearly observed in $x = 0.15$ and 0.19 (Fig. 13).

The present study reveals the phase separation in addition to the charge order as a nature of the transition at 220 K. It cannot be expected that the phase separation accompanied with a diffusion of oxygen atoms occurs at such low temperature (220 K). Therefore, the two phases should have the same composition (oxygen content). The O-phase (major phase) shows a similar temperature dependence of the lattice parameters to that reported before (8). This suggests that the O-phase has the same charge-ordered manner as that reported in Ref. (8), that is, Co^{2+}/Co^{3+} charge ordering into $Co^{2+}O_5$ chains running parallel to [010] but alternating with $Co^{3+}O_5$ chains along the a- and c-axes. These Co^{2+} and Co^{3+} chains alternating along the a-axis enhance the orthorhombic distortion. On the other hand, the T-phase is tetragonal and has much longer c-axis than that of the O-phase, as mentioned above. This might indicate another charge-ordered manner in the T-phase, for instance an alternating stacking of $Co^{2+}O_2$ and $Co^{3+}O_2$ planes along the c-axis. In such case, the phase separation might occur to relax the lattice distortion caused by the charge ordering. In any case, the phase separation simultaneously occurs with the charge order transition in $x = 0.00$. This is the first observation of macroscopic phase separation originating in charge ordering, although a microscopic phase separation has been reported in manganese and copper oxides. The macroscopic phase separation was observed in La_2CuO_{4+x} (12–15), but it was a phase separation into oxygen-rich and oxygen-poor phase. Apparently, the phase separation in $x = 0.00$ is not the case.

SUMMARY

We summarized the results in Fig. 14 as a phase diagram. $YBaCo_2O_{5+x}$ shows various kinds of phase transitions.

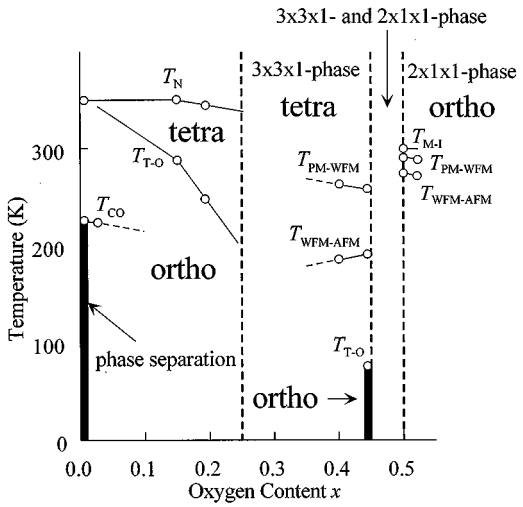

FIG. 14. Phase diagram of $YBaCo_2O_{5+x}$.

The $2 \times 1 \times 1$ phase shows the M-I transition accompanied with the lattice distortion and the magnetic transitions. The one-dimensional arrangement of oxygen atoms in $Y(O)_x$ layer is responsible for a quasi-metallic behavior in $YBaCo_2O_{5+x}$ ($x = 0.50$). The Co atoms have both octahedral and square pyramidal coordination in the $2 \times 1 \times 1$ phase; nevertheless, the average valence of Co ions is 3.0 + at the stoichiometric composition ($x = 0.50$). These phase transitions could be related to such imbalance between the charge/spin state and local structure or oxygen-coordination.

The $3 \times 3 \times 1$ phase lies in the range $0.25 \leq x \leq 0.44$. A plausible model of the $3 \times 3 \times 1$ superstructure is proposed (see Fig. 5a). At the stoichiometric composition $x = \frac{4}{9} = 0.44$, $\frac{4}{9}$ ($\frac{5}{9}$) of Co atoms has sixfold octahedral coordination (fivefold square pyramidal coordination), and the average valence of Co ions is 2.94 +. The stoichiometric $3 \times 3 \times 1$ phase shows a similar magnetic behavior as that of the $2 \times 1 \times 1$ phase but does not show any M–I transition.

In the range $0.00 \leq x \leq 0.19$, $YBaCo_2O_{5+x}$ has no longer superstructure. The Co atoms in $x = 0.00$ have only fivefold square pyramidal coordination but the average valence of 2.5 + ($Co^{2+}/Co^{3+} = 1$). Therefore, one may expect a charge order transition. However, the PM-AFM and T–O transitions occur accidentally at the same temperature first of all, holding a random distribution of Co^{2+} and Co^{3+}, and then a Co^{2+}/Co^{3+} charge ordering occurs in the antiferromagnetically ordered state at lower temperature (8). The PM-AFM transition occurs independently of the T–O transition in the nonstoichiometric $YBaCo_2O_{5+x}$. The present study reveals a simultaneous phase separation with the charge order transition. This is the first observation of macroscopic phase separation originating in charge

ordering. We are now planing an ED study to elucidate this charge order transition and simultaneous phase separation.

Further knowledge on the physical and structural properties needs a growth of single crystal and measurements that can make the microscopic observation of the magnetic structure such as NMR and neutron scattering.

ACKNOWLEDGMENTS

The authors thank Dr. Hiroshi Kageyama, Dr. Masahiko Isobe, Mr. Tohoru Yamauchi, and Dr. Jun-Ichi Yamaura of ISSP, University of Tokyo, and Prof. Noriaki Nakayama of Yamaguchi University for experimental support and helpful advice.

REFERENCES

1. W. Zhou, C. T. Lin, and W. Y. Liang. *Adv. Mater*. **5,** 735 (1993).
2. W. Zhou, *Chem. Mater*. **6,** 441 (1994).
3. D. Akahoshi and Y. Ueda, *J. Phys. Soc. Jpn.* **68,** 736 (1999).
4. C. Martin, A. Maignan, D. Pelloquin, N. Nguyen, and B. Raveau, *Appl. Phys. Lett*. **71,** 1421 (1997).
5. A. Maignan, C. Martin, D. Pelloquin, N. Nguyen, and B. Raveau, *J. Solid State Chem.* **142,** 247 (1999).
6. I. O. Troyanchuk, N. V. Kasper, D. D. Khalyavin, H. Szymczak, R. Szymczak, and M. Baran, *Phys. Rev. Lett*. **80,** 3380 (1998).
7. I. O. Troyanchuk, N. V. Kasper, D. D. Khalyavin, H. Szymczak, R. Szymczak, and M. Baran, *Phys. Rev. B* **58,** 2418 (1998).
8. T. Vogt, P. M. Woodward, P. Karen, B. A. Hunter, P. Henning, and A. R. Moodenbaugh, *Phys. Rev. Lett*. **84,** 2969 (2000).
9. S. Yamaguchi, H. Taniguchi, H. Takagi, T. Arima, and Y. Tokura, *J. Phys. Soc. Jpn.* **64,** 1885 (1995).
10. R. Mahendiran and A. K. Raychaudhuri, *Phys. Rev. B* **54,** 16044 (1996).
11. R. Mahendiran, A. K. Raychaudhuri, A. Chainani, and D. D. Sarma, *J. Phys. Condens. Matter* **7,** 4561 (1995).
12. J. D. Jorgensen, B. Dabrowski, Shiyou Pei, D. G. Hinks, L. Soderholm, B. Morosin, J. E. Schirber, E. L. Venturini, and D. S. Ginley, *Phys. Rev. B* **38,** 11337 (1988).
13. C. Chaillout, S. W. Cheong, Z. Fisk, M. S. Lehmann, M. Marezio, B. Morosin, and J. E. Schirber, *Physica C* **158,** 183 (1989).
14. C. Chaillout, J. Chenavas, S. W. Cheong, Z. Fisk, M. Marezio, B. Morosin, and J. E. Schirber, *Physica C* **170,** 87 (1990).
15. Y. Ueda, Y. Fujiwara, A. Hayashi, K. Shibutani, and R. Ogawa, *Physica C* **198,** 237 (1992).